

Showcasing research from the Centro de Nanotecnología Aplicada, Universidad Mayor, Chile, from the Center for the Development of Nanoscience and Nanotechnology CEDENNA, Chile and from the Universidad de Chile, Chile

Growth of Ni nanoclusters on irradiated graphene: a molecular dynamics study

This paper reports the soft landing of Ni clusters on a previously irradiated graphene sheet. The high diffusion of Ni on graphene together with the strong attachment of Ni atoms to vacancies induces unusual growing of nanoparticles, their probability of occurrence monotonically decreases with the nanoparticle size. A simple model was presented to explain this behavior and to generalize the results. The findings of this work show that a simple study of the energetics of this system is not enough, where it is unavoidable to also consider the growth process of metal clusters.

As featured in:





See F. Muñoz *et al.*,  
*Phys. Chem. Chem. Phys.*,  
2018, 20, 16347.



Cite this: *Phys. Chem. Chem. Phys.*,  
2018, 20, 16347

# Growth of Ni nanoclusters on irradiated graphene: a molecular dynamics study

F. J. Valencia,<sup>b,cf</sup> E. E. Hernandez-Vazquez,<sup>d</sup> E. M. Bringa,<sup>e</sup> J. L. Moran-Lopez,<sup>d</sup>  
J. Rogan,<sup>bc</sup> R. I. Gonzalez <sup>ac</sup> and F. Munoz <sup>\*bc</sup>

We studied the soft landing of Ni atoms on a previously damaged graphene sheet by means of molecular dynamics simulations. We found a monotonic decrease of the cluster frequency as a function of its size, but few big clusters comprise an appreciable fraction of the total number of Ni atoms. The aggregation of Ni atoms is also modeled by means of a simple phenomenological model. The results are in clear contrast with the case of hard or energetic landing of metal atoms, where there is a tendency to form mono-disperse metal clusters. This behavior is attributed to the high diffusion of unattached Ni atoms, together with vacancies acting as capture centers. The findings of this work show that a simple study of the energetics of the system is not enough in the soft landing regime, where it is unavoidable to also consider the growth process of metal clusters.

Received 26th December 2017,  
Accepted 3rd April 2018

DOI: 10.1039/c7cp08642c

rsc.li/pccp

## 1 Introduction

Besides the inherent mechanical and electronic properties of graphene,<sup>1,2</sup> some of its most promising aspects include the presence of defects such as vacancies or adatoms. This feature opens a door to a huge range of possibilities to tailor the already remarkable graphene properties.<sup>3,4</sup> In particular, the deposition of metallic atoms has been proposed as a way to improve the catalytic properties<sup>5–7</sup> of graphene and has also been suggested as a promising candidate for energy storage<sup>8</sup> and signal transduction.<sup>9</sup> However, metal clusters interact weakly with graphene<sup>10</sup> leading to the agglomeration and formation of large structures, with high diffusivity of metal atoms on graphene,<sup>11</sup> and the decrease of catalytic activity by cluster agglomeration.

Among the strategies to anchor metal clusters to a graphene sheet, the creation of Moire's patterns<sup>12,13</sup> between the substrate and the graphene layer produces mono-disperse and equally spaced clusters. Similarly, it has been observed that defects on the substrate supporting graphene can pin metal

adatoms on a graphene layer, leading to the growth of independent metal nanoislands.<sup>14</sup> However, there is another, less studied, option to pin metal adatoms over a graphene sheet: using graphene vacancies.<sup>15</sup>

Indeed, single vacancies can drastically affect the aggregation and nucleation processes and the growth of metal clusters on a graphene sheet.<sup>16</sup> Due to the defect's dangling bonds the cluster is strongly pinned to this position, preventing its diffusion, in an immense temperature range.<sup>17,18</sup>

One possibility to achieve the desired single vacancies on the graphene sheet is by bombarding it with energetic metal clusters (energetic landing). In this case the metal clusters damage the graphene sheet upon impacting, removing C atoms. Thus, the metallic clusters are attached to the produced defects.<sup>19–22</sup> If the freestanding clusters are mono-disperse in size, they are likely to remain mono-disperse on graphene.

Another possibility is to use a previously damaged graphene sheet,<sup>23</sup> together with the soft landing of the metal atoms. In fact, graphene with a given number of vacancies could be easily achieved<sup>24</sup> with ion beams<sup>25</sup> or microwave irradiation.<sup>26</sup> This procedure has been used to tailor its mechanical<sup>27</sup> and electrical properties.<sup>28</sup> Soft landing of metal atoms can be achieved by metal evaporation techniques,<sup>29</sup> resulting in the desired coverage of adatoms on graphene. This last and least studied case is the subject of this article. By means of molecular dynamics simulations and simple cluster growing phenomenological models, we study the behavior found in the soft landing of Ni atoms on already damaged graphene. We found marked differences with the energetic bombarding case. While the simulations only use Ni – because its interaction with graphene has been extensively studied,<sup>12,30</sup> our main

<sup>a</sup> Centro de Nanotecnología Aplicada, Facultad de Ciencias, Universidad Mayor, Santiago, Chile

<sup>b</sup> Departamento de Física, Facultad de Ciencias, Universidad de Chile, Santiago, Chile. E-mail: fvmunoz@gmail.com

<sup>c</sup> Centro para el Desarrollo de la Nanociencia y la Nanotecnología (CEDENNA), Santiago, Chile

<sup>d</sup> CONICET and Facultad de Ciencias Exactas y Naturales, Universidad Nacional de Cuyo, Mendoza, Argentina

<sup>e</sup> Advanced Materials Department, IPICYT, San Luis Potosí, San Luis Potosí, Mexico

<sup>f</sup> Núcleo de Matemáticas, Física y Estadística, Facultad de Ciencias, Universidad Mayor, Chile

conclusions are expected to remain valid for any 3d transition metal adatom.

## 2 Methods

### 2.1 Molecular dynamics simulations

To model the diffusion of Ni and the posterior growth of Ni clusters on graphene, we employed molecular dynamics (MD) simulations by means of the Large-scale Atomic/Molecular Massively Parallel Simulator (LAMMPS) code.<sup>31</sup> The interaction between C–C, Ni–Ni, and Ni–C atoms was modeled by using a reactive force field potential called ReaxFF.<sup>32</sup> An extensive description of this potential can be found elsewhere.<sup>32,33</sup> In this work we use the parameters for Ni/C interactions taken from the work of Yoon *et al.*,<sup>34</sup> trained against DFT simulations of spin-polarized phases of Nickel.<sup>35,36</sup> ReaxFF has successfully reproduced the interaction between a defective graphene sheet and Ni atoms among other Ni–C interfaces.<sup>37–40</sup> ReaxFF predicts the hole (six-fold coordinated) absorption site to be the most stable for a Ni atom over pure graphene, with an energy barrier of 0.08 eV. DFT predicts the hole site to be the most stable, but there is no agreement on the diffusion barrier with values ranging from 0.05 to 0.40 eV.<sup>41–43</sup> For defected graphene, the binding energy of Ni to single vacancies obtained by ReaxFF is 3.6 eV, while from DFT calculations it is estimated to be 6.9 eV.<sup>44</sup> Although this energy difference is large, it should not affect the dynamics of the system. As an additional test, we calculated the binding distance between a Ni<sub>10</sub> cluster and a graphene sheet, obtaining 0.214 nm with PBE+DF3, which includes van der Waals (vdW) corrections,<sup>45–49</sup> which is equal to the experimental distance for graphene grown on Ni(111).<sup>50</sup> As a comparison, PBE+DF2<sup>51</sup> underestimates this distance by 6%. ReaxFF overestimates this distance by 4% and, therefore, seems to lie within the acceptable margin of error of vdW corrected DFT calculations.

First, we generate a graphene sheet with periodic boundary conditions (PBC) along the *xy* plane and free along the *z* axis using the VMD code.<sup>52</sup> The size of the pristine graphene sheet is 10.2 × 10.3 nm and includes 3936 C atoms. Irradiated graphene sheets were simulated by randomly removing C atoms until the desired porosity,  $\theta_d$ , was obtained. To keep the analysis as simple as possible we generate only monovacancies, no more complex defects were included as Stone–Wales, divacancies, *etc.* Afterwards, the graphene layer was optimized using conjugate gradient optimization, relaxing both the atoms and the length of the simulation box along the PBC. Then, the system is connected to a zero pressure barostat and a 2500 K thermostat, to allow the simulation box to accommodate the vacancies for 0.2 ns. Using this procedure graphene samples with  $\theta_d = 0.25, 0.5, 0.75$  and 1.0% of vacancies were created, *i.e.* 10, 20, 30 and 40 monovacancies. The Ni atoms are deposited over graphene every 5 ps in a safe zone between 1.0 Å and 2.5 Å above the sheet, with a time-step of 0.5 fs. Using this procedure graphene is not damaged by Ni deposition and we avoid any heating due to the fast deposition range. Diffusion of Ni in graphene was simulated using a Nosé–Hoover thermostat.

Different deposition rates were studied. However, inserting a Ni atom every 5 ps is slow enough to avoid cluster formation before pinning to a vacancy. Finally, once all Ni atoms have been deposited, the system evolution is followed for at least 2.0 ns. To study the thermal behavior on Ni cluster formation we employed temperatures of  $T = 600, 700, 800, 1000, 1200, 1400, 1600,$  and 1800 K. There are experimental studies of diffusion of metal clusters on graphene up to 1000 K.<sup>53</sup> Above 1000 K, Ni clusters could decompose a graphene sheet,<sup>54</sup> but this is not the case for our simulations, where we employ very high temperatures to accelerate the rate of diffusive events without affecting the integrity of graphene.

### 2.2 Simple model for cluster growth

To model this system we follow a similar reasoning to the point island model, elegantly introduced by Bartelt and Evans.<sup>55</sup> However, since the fundamental interactions here are very different from the ones in the standard point island model, we reformulate it to reproduce the behavior observed in the MD simulations. In this respect, Appy *et al.*<sup>56</sup> studied the influence of defects on the heterogeneous nucleation of clusters.

There are three relevant processes involved in soft landing:

- Diffusion of free atoms on graphene. Activation energy for this process in the case of Ni is  $E_d = 0.05$  eV; for other 3d metals it ranges from almost nothing to 0.4 eV.<sup>57</sup>
- Diffusion of metal atoms from a vacancy. The binding energy of Ni (or any 3d metal) to a vacancy  $E_v$  is at least  $E_v = 6$  eV.<sup>44</sup>
- The disintegration of Ni clusters (already anchored to a vacancy) can be estimated by the binding energy of its dimer, Ni<sub>2</sub>,  $E_b = 3.5$  eV, for other 3d metals this energy ranges from  $E_b = 1.6$  (Mn<sub>2</sub>) to 5.9 eV (Ti<sub>2</sub>), averaging 3.5 eV for the 3d series.<sup>58</sup>

The Arrhenius equation can be employed to relate the rate of these events with their relevant energies at a given temperature. The diffusion coefficient is then

$$D = ga^2\nu_0 e^{-\frac{E_k}{T}}$$

where  $g$  is a geometrical factor of order 1,  $a$  is the lattice constant,  $\nu_0$  is the attempt frequency, and  $E$  is the activation energy. We can estimate the prefactor by using experimental data of a related system.<sup>53</sup>

From Table 1 we can see that the Boltzmann factor is the key to decouple diffusion processes into two very different temporal scales, slow and fast. While the slow scale is too slow to be of experimental concern, the fast scale is too fast to be experimentally observed by typical Transmission Electron Microscopy

**Table 1** Activation energies of relevant processes: diffusion of free atoms, diffusion from a vacancy, and from a cluster. Associated Boltzmann factors and diffusion coefficients are given at  $T = 1000$  K

$E$ (eV)	Boltzmann factor	$D$ (m s <sup>-2</sup> )
$E_d = 0.05$	$0.5 \times 10^0$	$1 \times 10^{-8}$
$E_v = 6.0$	$5.7 \times 10^{-31}$	$4 \times 10^{-39}$
$E_b = 3.5$	$2.3 \times 10^{-18}$	$3 \times 10^{-26}$

(TEM) measurements. An error in the estimation of the pre-factor – such as using the same attempt frequency for all processes – is effectively irrelevant. A couple of high-resolution TEM studies show this decoupling of the timescale of different processes, showing that while some events are too fast to be accounted, others have a diffusion coefficient close to  $1 \text{ nm s}^{-1}$ , and finally other processes are not observed during the experiment.<sup>53,59</sup>

The previous analysis holds for a large range of temperatures, but if we restrict ourselves to relatively high temperatures ( $T \sim 1000 \text{ K}$ ), and a low deposition rate ( $r$ ), then a Ni atom can travel a long distance between deposition events, and since those events are well separated in time, the formation of unattached clusters is very unlikely; thus we can ignore such a possibility. This intuitive observation has been corroborated by the MD simulations.

A concentration of defects of  $\theta_d \sim 1\%$  is small enough to ignore the coalescence among Ni islands without compromising the validity of the model. Another effect of this assumption is that the cross-section of the larger cluster can be an important fraction of the total area considered in the simulation.

Under the previous considerations, we propose the following simplified model: the probability of a wandering Ni atom to join a defect or cluster is proportional to its effective cross-section. This is the single most important effect to consider. It is even possible to ignore the underlying lattice since the metal atom can wander almost freely before randomly joining a vacancy.

Specifically, the probability of a free Ni atom to be attached to the cluster or defect  $i$  is given by:

$$P_i = \frac{A_i}{\sum_j A_j}, \quad (1)$$

where  $A_i$  is the effective area of the  $i$ -th cluster. For simplicity we assumed that the shape of the cluster is a half-sphere. Specifically we used  $A_i = \pi r_i^2$ , with  $r_i = \sqrt[3]{\frac{3n}{8\pi}}a + r_c$ , where  $n$  is the number of atoms of the cluster,  $a$  is the lattice parameter of bulk Ni, and  $r_c$  is the distance for which the vacancy or nanoisland can catch wandering atoms. In practice,  $r_c$  is the only free parameter.

The rate-equations for the number of cluster with  $s$  atoms,  $n_s$ , are:

$$\frac{dn_s}{dt} = rn_{s-1} \frac{A_{s-1}}{\sum_j A_j}, \quad (2)$$

where  $r$  is the deposition rate, which can be taken as unity without losing generality (we already excluded nucleation between wandering atoms). Finding an analytical solution of this set of equations is beyond the scope of the current study. However, it is easy to infer that, once the size of a cluster is large enough  $\left(A_i \sim \sum_j A_j\right)$ , a large fraction of the deposited Ni atoms will attach to it. Then, a strongly inhomogeneous cluster

size distribution is to be expected. Bigger clusters get bigger at a much faster pace than smaller ones. These equations can be solved within the framework of a Monte Carlo (MC) model,<sup>60</sup> for different initial distributions of vacancies and metal atoms.

### 3 Results

In Fig. 1 we illustrate the soft landing process of 200 Ni atoms on a graphene sheet with a porosity  $\theta_d = 0.5\%$  (21 vacancies) at 800 K. As shown in Fig. 1a, just a fraction of a nanosecond is required for Ni atoms to attach to a vacancy or to form clusters. As expected, the formation of dimers and trimers starts when the Ni coverage is comparable to the number of graphene vacancies. The high mobility of Ni on graphene is similar to other metallic atoms, such as Pt and Au whose relevant energies are similar,<sup>61,62</sup> despite their much smaller binding energy to graphene. When Ni atoms are pinned to vacancies they remain there, even at temperatures close to 2000 K, acting as seeds for the growth of larger Ni clusters. Fig. 1d illustrates a set of representative small clusters ranging from  $\text{Ni}_4$  to  $\text{Ni}_{13}$ . Those clusters have the typical growing pattern found on freestanding  $\text{Ni}_n$  clusters,<sup>63</sup> despite their strong binding to a vacancy. One of the most striking characteristics of atomic clusters – especially in the gas phase – is the abundance of some clusters with a specific number of atoms; these clusters are more stable than the rest and are denominated as “magic clusters”. In simple metals such as Li, magic clusters appear when the number of electrons closes a shell of angular momentum,<sup>64</sup> while more complex elements – such as transition metals – also have magic clusters but it is much harder to predict why a specific cluster is magic. In a standard growth process where nucleation and decomposition of clusters are relevant, we would have expected an abundance peak at some magic numbers, but this is not the case for the regime of soft landing on a graphene sheet with single vacancies studied here.

With the deposition rate used in our simulations, the formation of dimers, trimers or larger clusters away from a vacancy is a very rare event. Diffusivity of (unattached) dimers is

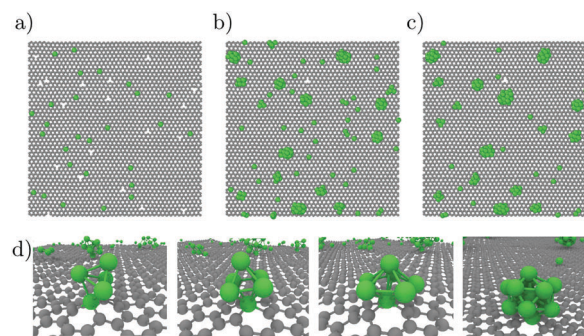


**Fig. 1** Coverage of the graphene surface during the first few ps of simulation; green and gray atoms correspond to Ni and C, respectively. Panels (a–c) show the graphene surface after the deposition of 40, 140 and 200 Ni atoms, respectively. In panel (d) we show the first stages of the growth of some clusters,  $\text{Ni}_5$ ,  $\text{Ni}_6$ ,  $\text{Ni}_7$  and  $\text{Ni}_{13}$ . The porosity is  $\theta_d = 0.5\%$  and  $T = 800 \text{ K}$ .

even larger than that of single Ni atoms, preventing the formation of unattached islands. At first glance this may seem counter-intuitive, but when two Ni atoms form a bond its potential energy drops by  $\sim 1$  eV, increasing the dimer kinetic energy, and hence its mobility. Eventually the unattached dimer must thermalize, but its mean free path (before finding a vacancy) is shorter. Despite the large wealth of studies on graphene, there are few articles on the diffusion of metal atoms on graphene and this subject deserves more attention.

As observed in Fig. 1c, the size-distribution of Ni clusters on graphene is not homogeneous at all. This behavior is opposed to the case of 'hard-landing' of metal atoms. Therefore, we need to study the clustering process in more detail. The average cluster size does not provide much information since it is just the ratio between Ni atoms to occupied vacancies. However, if we ignore the monomers from the average, we can obtain some insights into the system's tendency to form big clusters.

The previously defined average (excluding monomers) is shown in Fig. 2a for two relevant times: in the middle of the nucleation process ( $t = 1.1$  ns), and after it has finished ( $t = 2.0$  ns, *i.e.* when all Ni atoms are pinned to vacancies). This average size,  $N$ , increases almost linearly with the temperature  $T$ , starting the nucleation at early stages of the deposition process. The long-time curve in Fig. 2a shows a clear tendency to form bigger clusters at larger  $T$ . Indeed, as soon as a cluster becomes big enough, its cross section allows it to trap wandering Ni atoms, to the detriment of

the nucleation on free vacancies or smaller clusters. Another effect of the temperature rise is an increase in the mean free path of the metal atoms. To understand this behaviour we note that a point defect in graphene behaves as a potential well with a radius of around 1.5 nm, but beyond 0.5 nm this potential well is very shallow,<sup>65</sup> and thermal energy can prevent metal atoms from falling into the deeper region of the well, in the same way as the temperature helps with regular diffusion. In this way temperature favors the formation of few bigger nanostructures. Those resulting clusters are highly disperse in size. From these data ( $t = 2.0$  ns) we fitted the only free parameter of our Monte Carlo model for each temperature, obtaining  $r_c$  in the range 0.7–1.25 Å. Beyond  $t = 2.0$  ns no diffusion event was observed, see Fig. 2d and e. After that time the average cluster size and the number of monomers remain constant, which is consistent with the discussion about the diffusion timescale from the previous section.

At temperatures of 1400 K or more, it is common to find clusters whose size is different from the general trends; a single cluster may contain about 40% of all the Ni atoms, see Fig. 3. Even though it would be desirable to show the histograms obtained from the averaging of several MD simulations, due to the inherent out-of-equilibrium dynamical process, this would require thousands of simulations to obtain smooth averages. Furthermore, the averaging would veil the fundamental physics. This is because a large fraction of the atoms are in few big clusters (see Fig. 3), and the size of those clusters varies significantly from simulation to simulation, making its frequency almost negligible, nearly vanishing for an averaged histogram. With the help of our simple MC model, we calculated the average frequency for each cluster size, which seems to show a tendency to have mostly smaller clusters, but this is due the small frequency of each (big) cluster size. Inspection of the results of the MC runs prior to averaging shows qualitative agreement with our MD simulations.

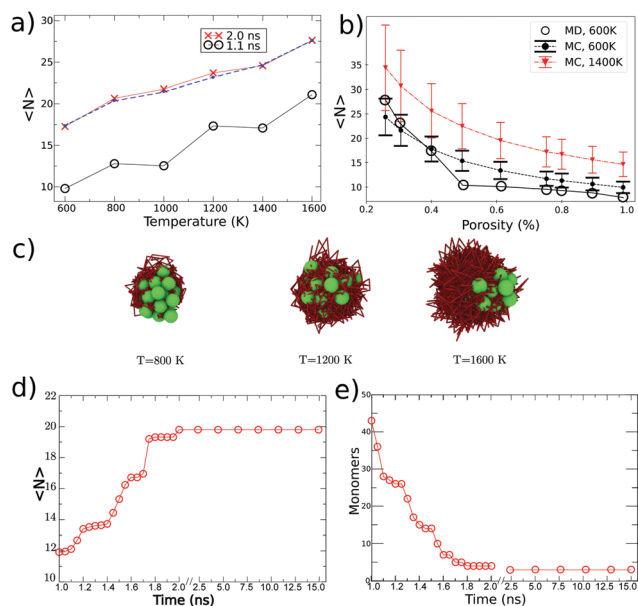


**Fig. 2** (a) Average cluster size (number of atoms) as a function of the temperature for two representative instants and a porosity of  $\theta_d = 0.4\%$ . The dashed lines are fits to the Monte Carlo (MC) model. (b) Average numbers of atoms per cluster for different porosities ( $\theta_d$ ) of graphene and  $T = 600$  K. Results from MC simulations include their standard deviation. Only clusters with  $N \geq 2$  were considered. (c) Trajectory lines at different temperatures for a representative  $N_{23}$  cluster pinned to a vacancy. The cluster diameters are 10.5, 10.9 and 12.9 Å according to  $T$ . (d and e) Average cluster size and number of monomers as a function of time for  $T = 800$  K and  $\theta_d = 0.4\%$ .

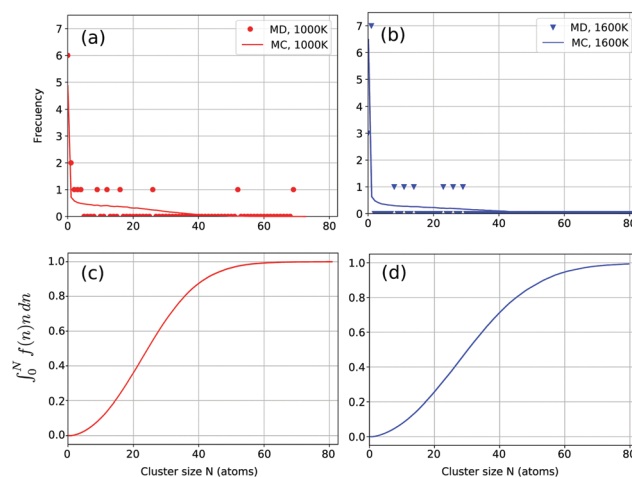


**Fig. 3** (a and b) Histograms of the cluster frequency as a function of their size. The temperatures are 1000 and 1600 K. The porosity is  $\theta_d = 0.4\%$ . The zero-size clusters stand for empty vacancies. Each histogram is a MD simulation, without averaging. The continuous line is the average obtained using the Monte Carlo model. The panels (c and d) show the weighted cumulative frequency for each cluster size, that is, the probability of having a cluster of size  $N$  or smaller.

A better indicator of the occurrence of bigger clusters is the weighted cumulative frequency, which is simply the probability of having a cluster of size  $N$  or smaller, see Fig. 3c and d. For  $T = 1000$  K  $\sim 90\%$  of the metal atoms belong to clusters with 40 atoms or less, considering a total of 200 metal atoms. Conversely, there are 10% of the atoms which form part of clusters with at least 40 atoms. For  $T = 1600$  K, nearly 30% of the metal atoms belong to clusters with 40 atoms or more. The monotonous decrease of the frequency of clusters as a function of their size seems to be a general consequence of defects on the substrate.<sup>56</sup>

The other parameter affecting the growth dynamics of the clusters is the porosity  $\theta_d$ . As this parameter increases, the mean free path decreases, making the nucleation on a vacancy easier and inhibiting the nucleation of few big clusters; see Fig. 2b. Given the large computational cost of each MD simulation, it is impractical to average several MD simulations. However, it is cheap to use our MC model to get insights into the behavior of the porosity, including the standard deviation of the data (errors bars in Fig. 2b). While we obtain that the average size smoothly decreases with porosity, its dispersion is very large, specially for the limit of low porosity and high temperatures, in line with our previous findings. It is worth noting that a porosity of  $\theta_d = 0.5\%$  means that 1% of the unit cells and 3% of the hexagons of graphene are damaged.

Therefore, under experimental conditions there are two important parameters controlling the aggregation behavior: graphene temperature and its porosity. A large  $T$  helps having fewer and bigger clusters, but the increment of  $\theta_d$  has the opposite effect. When the temperature reaches  $\sim 1600$  K the kinetic energy of the clusters allows them to move almost freely around the vacancy (but without breaking off), see Fig. 2c, making its cross section a circle of diameter close to  $2d$ , with  $d$  being the Ni cluster diameter. This last effect increases the tendency to form larger clusters even further.

## 4 Conclusions

Graphene is an extremely interesting material with technological applications. Small changes can lead to enormous effects, like the recently presented case of superconductivity when one sheet is rotated over other by less than 2 degrees.<sup>66</sup> Another example is the doubling of the elastic modulus thanks to the presence of about 0.1% vacancy concentration.<sup>24</sup>

Here we present simulation results on how to decorate graphene with metallic clusters, controlling their size and distribution *via* single vacancy concentration and temperature. Such nano-architecturing of graphene might help in understanding future experiments, and might lead to unexpected technological applications.

We have studied the soft landing of Ni atoms on an already damaged graphene layer. We find marked differences as compared to the case of hard landing of the metal cluster and to the adsorption over a undamaged graphene sheet. The most important aspects of the soft landing are as follows:

- The binding energy of adatoms or clusters adhered to a vacancy is very large, preventing their migration even at  $T \sim 2000$  K.
- There is a marked tendency to have a few big clusters. Those clusters have a significant fraction of the total number of Ni atoms.
- Unlike the case of homogeneous nucleation, the frequency of clusters as a function of their size is a monotonous decreasing function.
- Higher values of the porosity (vacancies) of the graphene layer decrease the mean free path of wandering Ni atoms, preventing the formation of the aforementioned larger clusters.
- Higher values of temperature increase the mean free path of wandering Ni atoms making them more likely to form a few big clusters.
- Due to the large difference between the relevant diffusion energies, the so-called magic clusters are not expected to be prevalent on a damaged graphene sheet.

We made an idealized model for the evolution of cluster sizes, solved within a Monte Carlo framework, which is able to capture the previous behavior, in excellent agreement with molecular dynamics, with a single free parameter. The model is expected to remain valid for any 3d transition metal species<sup>67</sup> making our conclusions rather general.

We want to emphasize that defects and adatoms in graphene modify mechanical properties non-trivially, modifying its roughness.<sup>24,68</sup> The influence of roughness on clustering and defect diffusion is beyond the scope of this paper, partly because, in order to capture typical length-scales associated with graphene roughness, we would have to use samples more than two orders of magnitude larger than the ones presented here.

Future simulations might include other typical defects, including vacancy clusters and grain boundaries, with different diffusivity time-scales which may require significantly more computational resources.

In summary, tuning the size distributions of metal atom clusters on graphene is possible *via* temperature and single vacancy concentration variations. This might help in obtaining desired chemical and mechanical properties for sensors,<sup>69</sup> and optoelectronic properties for future devices.<sup>2</sup>

## Conflicts of interest

There are no conflicts to declare.

## Acknowledgements

Support from the following sources is acknowledged: Fondecyt (Chile) under contracts 1150806, 1160639 and Financiamiento Basal para Centros Científicos y Tecnológicos de Excelencia (Chile) through the Center for Development of Nanoscience and Nanotechnology (CEDENNA, Contract FB0807). E. E. H.-V. acknowledges a fellowship from CONACYT, contract 288363 (Mexico). This research was partially supported by the super-computing infrastructure of the NLHPC (ECM-02). E. M. Bringa

is thankful for the support from grants PICT2014-0096 and SeCTyP-UNCuyo M025.

## References

- 1 A. H. Castro Neto, F. Guinea, N. M. R. Peres, K. S. Novoselov and A. K. Geim, *Rev. Mod. Phys.*, 2009, **81**, 109–162.
- 2 X. Li, L. Tao, Z. Chen, H. Fang, X. Li, X. Wang, J.-B. Xu and H. Zhu, *Appl. Phys. Rev.*, 2017, **4**, 021306.
- 3 P.-H. Ho, Y.-T. Liou, C.-H. Chuang, S.-W. Lin, C.-Y. Tseng, D.-Y. Wang, C.-C. Chen, W.-Y. Hung, C.-Y. Wen and C.-W. Chen, *Adv. Mater.*, 2015, **27**, 1724–1729.
- 4 H. Sevinçli, M. Topsakal, E. Durgun and S. Ciraci, *Phys. Rev. B: Condens. Matter Mater. Phys.*, 2008, **77**, 195434.
- 5 M. Zhou, Y.-H. Lu, Y.-Q. Cai, C. Zhang and Y.-P. Feng, *Nanotechnology*, 2011, **22**, 385502.
- 6 S. Sun, G. Zhang, N. Gauquelin, N. Chen, J. Zhou, S. Yang, W. Chen, X. Meng, D. Geng and M. N. Banis, *et al.*, *Sci. Rep.*, 2013, **3**, 1775.
- 7 Y. Tang, Z. Lu, W. Chen, W. Li and X. Dai, *Phys. Chem. Chem. Phys.*, 2015, **17**, 11598–11608.
- 8 M. Gaboardi, A. Bliersbach, G. Bertoni, M. Aramini, G. Vlahopoulou, D. Pontiroli, P. Mauron, G. Magnani, G. Salviati and A. Züttel, *et al.*, *J. Mater. Chem. A*, 2014, **2**, 1039–1046.
- 9 A. V. Zaretski, S. E. Root, A. Savchenko, E. Molokanova, A. D. Printz, L. Jibril, G. Arya, M. Mercola and D. J. Lipomi, *Nano Lett.*, 2016, **16**, 1375–1380.
- 10 K. T. Chan, J. B. Neaton and M. L. Cohen, *Phys. Rev. B: Condens. Matter Mater. Phys.*, 2008, **77**, 235430.
- 11 H. Wang, K. Li, Y. Yao, Q. Wang, Y. Cheng, U. Schwingenschlögl, X. X. Zhang and W. Yang, *Sci. Rep.*, 2012, **2**, 995.
- 12 A. Dahal and M. Batzill, *Nanoscale*, 2014, **6**, 2548–2562.
- 13 S. Bleikamp, P. J. Feibelman and T. Michely, *et al.*, *Phys. Rev. Lett.*, 2006, **97**, 215501.
- 14 J. Coraux, M. Engler, C. Busse, D. Wall, N. Buckanie, F.-J. M. Zu Heringdorf, R. Van Gastel, B. Poelsema and T. Michely, *et al.*, *New J. Phys.*, 2009, **11**, 023006.
- 15 H. Zhou, X. Chen, L. Wang, X. Zhong, G. Zhuang, X. Li, D. Mei and J. Wang, *Phys. Chem. Chem. Phys.*, 2015, **17**, 24420–24426.
- 16 W. Song, M. Jiao, K. Li, Y. Wang and Z. Wu, *Chem. Phys. Lett.*, 2013, **588**, 203–207.
- 17 A. W. Robertson, B. Montanari, K. He, J. Kim, C. S. Allen, Y. A. Wu, J. Olivier, J. Neethling, N. Harrison and A. I. Kirkland, *et al.*, *Nano Lett.*, 2013, **13**, 1468–1475.
- 18 J. A. Rodriguez-Manzo, O. Cretu and F. Banhart, *ACS Nano*, 2010, **4**, 3422–3428.
- 19 S. J. Carroll, S. Pratontep, M. Streun, R. E. Palmer, S. Hobday and R. Smith, *J. Chem. Phys.*, 2000, **113**, 7723–7727.
- 20 S. Gibilisco, M. D. Vece, S. Palomba, G. Faraci and R. E. Palmer, *J. Chem. Phys.*, 2006, **125**, 084704.
- 21 R. Smith, C. Nock, S. D. Kenny, J. J. Belbruno, M. Di Vece, S. Palomba and R. E. Palmer, *Phys. Rev. B: Condens. Matter Mater. Phys.*, 2006, **73**, 125429.
- 22 M. Di Vece, S. Palomba and R. E. Palmer, *Phys. Rev. B: Condens. Matter Mater. Phys.*, 2005, **72**, 073407.
- 23 Z. Li and F. Chen, *Appl. Phys. Rev.*, 2017, **4**, 011103.
- 24 G. López-Poln, C. Gómez-Navarro, V. Parente, F. Guinea, M. I. Katsnelson, F. Pérez-Murano and J. Gómez-Herrero, *Nat. Phys.*, 2015, **11**, 26–31.
- 25 J. Buchheim, R. M. Wyss, I. Shorubalko and H. G. Park, *Nanoscale*, 2016, **8**, 8345–8354.
- 26 R. Rozada, P. Solís-Fernández, J. I. Paredes, A. Martínez-Alonso, H. Ago and J. M. D. Tascón, *Carbon*, 2014, **79**, 664–669.
- 27 G. Rajasekaran, P. Narayanan and A. Parashar, *Crit. Rev. Solid State Mater. Sci.*, 2016, **41**, 47–71.
- 28 A. Krasheninnikov and F. Banhart, *Nat. Mater.*, 2007, **6**, 723–733.
- 29 V. Franchetti, B. Solka, W. Baitinger, J. Amy and R. Cooks, *Int. J. Mass Spectrom. Ion Phys.*, 1977, **23**, 29–35.
- 30 J. Li, E. Croiset and L. Ricardez-Sandoval, *Phys. Chem. Chem. Phys.*, 2014, **16**, 2954–2961.
- 31 S. Plimpton, *J. Comput. Phys.*, 1995, **117**, 1–19.
- 32 A. C. Van Duin, S. Dasgupta, F. Lorant and W. A. Goddard, *J. Phys. Chem. A*, 2001, **105**, 9396–9409.
- 33 K. Chenoweth, A. C. Van Duin and W. A. Goddard, *J. Phys. Chem. A*, 2008, **112**, 1040–1053.
- 34 K. Yoon, A. Ostadhossein and A. C. van Duin, *Carbon*, 2016, **99**, 58–64.
- 35 J. E. Mueller, A. C. T. van Duin and W. A. Goddard, *J. Phys. Chem. C*, 2010, **114**, 4939–4949.
- 36 K. D. Nielson, A. C. T. van Duin, J. Oxgaard, W.-Q. Deng and W. A. Goddard, *J. Phys. Chem. A*, 2005, **109**, 493–499.
- 37 L. Meng, J. Jiang, J. Wang and F. Ding, *J. Phys. Chem. C*, 2013, **118**, 720–724.
- 38 Y. Lu and X. Yang, *Carbon*, 2015, **81**, 564–573.
- 39 R. I. González, F. Valencia, J. Mella, A. C. van Duin, K. P. So, J. Li, M. Kiwi and E. M. Bringa, *Appl. Phys. Lett.*, 2016, **109**, 033108.
- 40 E. Neyts and A. Bogaerts, *Carbon*, 2014, **77**, 790–795.
- 41 A. Ishii, M. Yamamoto, H. Asano and K. Fujiwara, *J. Phys.: Conf. Ser.*, 2008, **100**, 052087.
- 42 M. Manadé, F. Viñes and F. Illas, *Carbon*, 2015, **95**, 525–534.
- 43 K. Nakada and A. Ishii, *Solid State Commun.*, 2011, **151**, 13–16.
- 44 A. V. Krasheninnikov, P. O. Lehtinen, A. S. Foster, P. Pyykkö and R. M. Nieminen, *Phys. Rev. Lett.*, 2009, **102**, 126807.
- 45 G. Kresse and J. Hafner, *Phys. Rev. B: Condens. Matter Mater. Phys.*, 1993, **47**, 558–561.
- 46 G. Kresse and J. Furthmüller, *Comput. Mater. Sci.*, 1996, **6**, 15–50.
- 47 G. Kresse and J. Furthmüller, *Phys. Rev. B: Condens. Matter Mater. Phys.*, 1996, **54**, 11169–11186.
- 48 J. P. Perdew, K. Burke and M. Ernzerhof, *Phys. Rev. Lett.*, 1996, **77**, 3865–3868.
- 49 S. Grimme, J. Antony, S. Ehrlich and H. Krieg, *J. Chem. Phys.*, 2010, **132**, 154104.
- 50 M. Batzill, *Surf. Sci. Rep.*, 2012, **67**, 83–115.
- 51 S. Grimme, *J. Comput. Chem.*, 2006, **27**, 1787–1799.

- 52 W. Humphrey, A. Dalke and K. Schulten, *J. Mol. Graphics Modell.*, 1996, **14**, 33–38.
- 53 Y. Gan, L. Sun and F. Banhart, *Small*, 2008, **4**, 587–591.
- 54 L. Campos, V. Manfrinato, J. Sanchez-Yamagishi, J. Kong and P. Jarillo-Herrero, *Nano Lett.*, 2009, **9**, 2600–2604.
- 55 M. C. Bartelt and J. W. Evans, *Phys. Rev. B: Condens. Matter Mater. Phys.*, 1992, **46**, 12675–12687.
- 56 D. Appy, H. Lei, C.-Z. Wang, M. C. Tringides, D.-J. Liu, J. W. Evans and P. A. Thiel, *Prog. Surf. Sci.*, 2014, **89**, 219–238.
- 57 X. Liu, C. Z. Wang, M. Hupalo, W. C. Lu, M. C. Tringides, Y. X. Yao and K. M. Ho, *Phys. Chem. Chem. Phys.*, 2012, **14**, 9157–9166.
- 58 M. Valiev, E. J. Bylaska and J. H. Weare, *J. Chem. Phys.*, 2003, **119**, 5955–5964.
- 59 O. Cretu, A. V. Krasheninnikov, J. A. Rodriguez-Manzo, L. Sun, R. M. Nieminen and F. Banhart, *Phys. Rev. Lett.*, 2010, **105**, 196102.
- 60 M. Allen and D. Tildesley, *Computer Simulation of Liquids*, Clarendon Pr, Oxford, 1987.
- 61 Y. Gan, L. Sun and F. Banhart, *Small*, 2008, **4**, 587–591.
- 62 R. N. Lenz Baldez, P. Piquini, A. A. Schmidt and M. A. Kuroda, *Phys. Chem. Chem. Phys.*, 2017, **19**, 22153–22160.
- 63 T. Futschek, J. Hafner and M. Marsman, *J. Phys.: Condens. Matter*, 2006, **18**, 9703.
- 64 M. Brack, *Rev. Mod. Phys.*, 1993, **65**, 677–732.
- 65 A. V. Krasheninnikov and R. M. Nieminen, *Theor. Chem. Acc.*, 2011, **129**, 625–630.
- 66 E. Gibney, *Nature*, 2018, **555**, 151–152.
- 67 D. Appy, H. Lei, C.-Z. Wang, M. C. Tringides, D.-J. Liu, J. W. Evans and P. A. Thiel, *Prog. Surf. Sci.*, 2014, **89**, 219–238.
- 68 J. Martinez-Asencio, C. J. Ruestes, E. M. Bringa and M. J. Caturla, *Phys. Chem. Chem. Phys.*, 2016, **18**, 13897–13903.
- 69 B. Arash, J.-W. Jiang and T. Rabczuk, *Appl. Phys. Rev.*, 2015, **2**, 021301.